Synthesis and Characterization of the Anionic Conductor System $La_2Mo_2O_{9-0.5x}F_x$ ($x = 0.02-0.30$)

A. Arulraj,*[,†,‡] F. Goutenoire,[‡] M. Tabellout,[§] O. Bohnke,[‡] and P. Lacorre[‡]

Laboratoire des Fluorures, UMR-CNRS 6010, and Laboratoire de Physique de l'Etat Condensé, UMR-CNRS 6087, Université du Maine, Av. Olivier Messiaen, 72085 Le Mans, France

Received September 14, 2001. Revised Manuscript Received March 7, 2002

Fluorine-doped lanthanum molybdates with the nominal formula $La_2Mo_2O_{9-0.5x}F_x$ ($x = 0.20-0.30$) were synthesized and characterized using powder X-ray diffraction, electron diffraction, differential thermal analysis, and impedance spectroscopy. Comparisons are made with the parent anionic conductor system $La_2Mo_2O_9$. From our studies two distinct regimes with two different ranges of "x" values (range 1: including $0.00 \le x \le 0.12$; range 2: including $0.18 \le x \le 0.30$) could be delineated for the $La_2Mo_2O_{9-0.5x}F_x$ compositions. Electron diffraction study on selected samples showed that $x = 0.20$ and 0.30 compositions (range 2) have a $3 \times 3 \times 3$ supercell, different from the $2 \times 3 \times 4$ supercell observed in the $x = 0.00$ and 0.10 compositions (range 1). All the fluorine-doped lanthanum molybdates show a first-order phase transition. With the increase in the fluorine content the transition temperature decreases in both ranges 1 and 2. Below the transition temperature, compositions belonging to range 2 have much lower conductivity when compared to that of those belonging to range 1. The activation energy as obtained from the conductivity data is higher for the fluorine-doped lanthanum molybdates compared to the parent compound $La_2Mo_2O_9$. Above the transition temperature the conductivity of the fluorine-doped lanthanum molybdate is higher than that of $La_2Mo_2O_9$. Significantly our study presents the possibility of using fluorine substitution as a technique to increase the anionic conductivity in oxide ion conductors with favorable structural features (like in the case of $La_2Mo_2O_9$) by decreasing the transition temperature of the first-order (order−disorder type) phase transition.

1. Introduction

Recently, a new family of fast oxide ion conductors called LAMOX with lanthanum molybdate $La_2Mo_2O_9$ as the parent compound was reported.[1] $La_2Mo_2O_9$ exhibits a first-order transition at around 580 °C where it transforms from a low-temperature α-form to a high-temperature β-form. Around the same temperature a jump in the conductivity is observed with a 2 orders of magnitude higher conductivity value for the high-temperature phase. The β-$La_2Mo_2O_9$ form has a cubic symmetry[2] (space group $P2_13$, $a = 7.2014$ Å) and the structure of the low-temperature α-$La_2Mo_2O_9$ is not known yet. Careful X-ray diffraction study indicated the presence of a monoclinic distortion. Electron diffraction studies showed the presence of a superlattice with a $2 \times 3 \times 4$ supercell. The reflections corresponding to this superlattice were also observed in the X-ray as well as neutron diffraction studies.[2] $La_2Mo_2O_9$ provides a striking example of a new concept called lone-pair substitution (LPS), which in principle could be used to design new anion conductors from already known ceramics.[3] Various substitutions on the cationic sites of $La_2Mo_2O_9$ have shown systematic trends in its crystallographic properties.[4] For instance, the partial substitution of La by cations with larger mean ionic radii, like Sr(II) and K(I), resulted in an increase in the pseudo cubic cell parameter at room temperature, while the substitution of Mo by cations with smaller mean ionic radii, like S(VI), Cr(VI), and V(V), resulted in the lowering of the room-temperature lattice parameter of the resulting phases. All these substitutions resulted in the stabilization of the high-temperature cubic structure of $La_2Mo_2O_9$ at room temperature. It is also possible to realize anionic substitution in $La_2Mo_2O_9$; for example, fluorine can be partially substituted for oxygen. The mean ionic size of O^{2-} (≈1.35 Å) and F^- (≈1.29 Å) are comparable.[5] For the charge neutrality considerations, on partial substitution each oxide (O^{2-}) ion will be replaced by two fluoride (F^-) ions. Following refs 1−4, $La_2Mo_2O_9$ can be represented as $La_2Mo_2O_{8+1}\square$, where □ represents a vacancy in the oxygen sublattice. A progressive substitution of oxygen by fluorine would lead to fluoride ions occupying the vacancy sites, thereby leading to a

* To whom correspondence should be addressed. E-mail: anthony.arulraj@uni-bayreuth.de.
† Present address: Laboratory of Crystallography, University of Bayreuth, Germany.
‡ Laboratoire des Fluorures, UMR-CNRS 6010.
§ Laboratoire de Physique de l'Etat Condensé, UMR-CNRS 6087.

(1) Lacorre, P.; Goutenoire, F.; Bohnke, O.; Retoux, R.; Laligant, Y. *Nature* **2000**, *404,* 856.
(2) Goutenoire, F.; Isnard, O.; Retoux, R.; Lacorre, P. *Chem. Mater.* **2000**, *12,* 2575.
(3) Lacorre, P. *Solid State Sci.* **2000**, *2,* 755.
(4) Goutenoire, F.; Isnard, O.; Suard, E.; Bohnke, O.; Laligant, Y.; Retoux, R.; Lacorre, P. J. *Mater. Chem.* **2001**, *11,* 119.
(5) Shannon, R. D. *Acta Crystallogr.* **1976**, *A32,* 751.

10.1021/cm011239x CCC: $22.00
Published on Web 05/15/2002

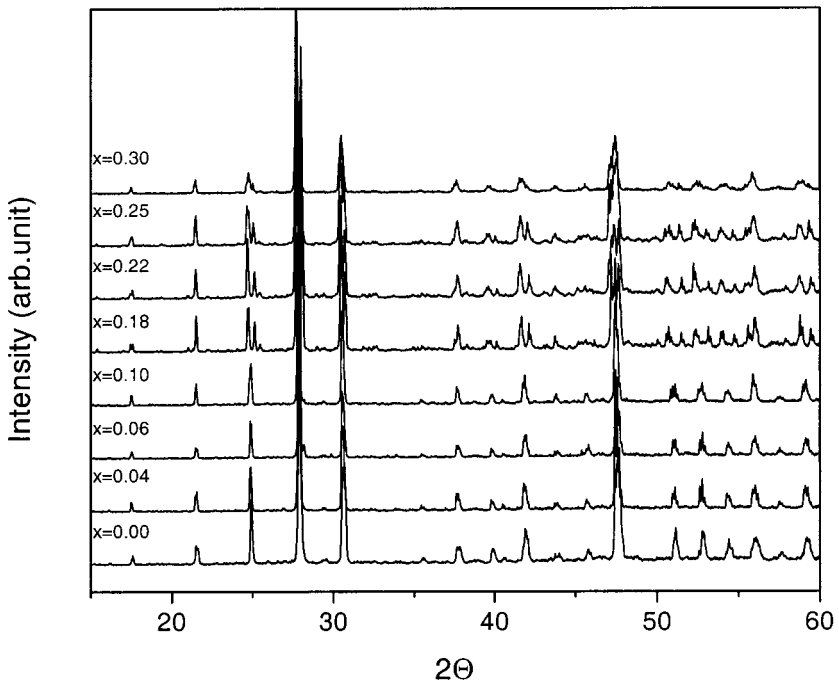

Figure 1. Evolution of the powder X-ray diffraction pattern of the $La_2Mo_2O_{9-0.5x}F_x$ system as the function of the fluorine content "*x*".

decrease in the number of vacancies in this model. Fluoride ions, owing to their size and charge (−1), could favor anionic conduction and it is plausible to expect interesting changes in crystallographic as well as transport properties of the $La_2Mo_2O_{9-0.5x}F_x$ system as a function of *x*. In this paper we report the results of our systematic study on the synthesis and characterization of the fluorine-doped lanthanum molybdate system $La_2Mo_2O_{9-0.5x}F_x$ ($x = 0.02-0.30$). Our attempts to synthesize the composition $La_2Mo_2O_8F_2$ resulted in the formation of a new phase and more study is being carried on it, which will not be covered in this article.

2. Experimental Section

All $La_2Mo_2O_{9-0.5x}F_x$ ($x = 0.02-0.30$) compositions were made from La_2O_3, MoO_3, and LaOF as starting materials. Stoichiometeric quantities of the starting materials were mixed thoroughly in an agate mortar and sealed in a platinum tube. The sealed Pt tube containing the mixture was first heated at 500 °C and then at 900 °C for 12 h each. The heating and cooling rate was maintained at 2°/min for all the heatings. LaOF itself was made by heating thoroughly mixed stoichiometric quantities of LaF_3 and La_2O_3 in a sealed Pt tube at 500 and 900 °C, respectively, for 12 h each. Weighing and mixing of LaF_3 and La_2O_3 were done in a dry N_2 atmosphere in a glovebox. For selected samples, thoroughly ground stoichiometric quantities of the raw material were palletized into rod-shaped pellets and sealed in Pt tubes. Sealed Pt tubes were subjected to heating conditions such as those of the powder samples. All $La_2Mo_2O_{9-0.5x}F_x$ compositions were white in color.

The X-ray powder diffraction data was recorded on a Bruker-AXS D8 diffractometer. The electron diffraction study was performed on a 200-kV side entry JEOL 2010 electron microscope with a double-tilt specimen holder operated at room temperature.

Differential thermal analysis (DTA) in a flowing Ar atmosphere was carried out using a DTA/TGA apparatus (SDT 2960, TA Instruments) and a heating and cooling rate of 15°/min was used.

The low-temperature impedance measurements were performed over a wide frequency range (0.1 Hz to 1.8 GHz) at temperatures between −150 and 350 °C using a Novocontrol Broadband Dielectric Spectrometer. The temperature was controlled within the accuracy of ±1 °C using a gas stream of nitrogen. To cover the frequency domain between 0.1 Hz and 1.8 GHz, two different measurement systems based on different measurement techniques were employed. From 0.1 Hz up to 10 MHz a Solartron SI1260 combined with a Broadband Dielectric Converter (BDC) was used and for the high-frequency range (1 MHz to 1.8 GHz) an HP4291A rf impedance analyzer was used with a precision coaxial line for which propagation parameters are well-defined. For both techniques the sample cell consisted of two round gold plate electrodes between which the sample was placed forming a capacitor. In the case of the high-frequency range the sample capacitor is used as the termination of a golden coaxial line and the impedance is then calculated from the complex reflection factor at the analyzer end of the line. For both techniques the sample temperature is measured in the immediate neighborhood of the sample with accuracy better than ±0.1. The high-temperature impedance spectra in the frequency range of 0.1−32 MHz was recorded using a Solartron SI1260 Frequency Response Analyzer in the temperature range 30−800 °C. The measurements were carried out under dry air at a potential of 100 mV (r.m.s).

Rod-shaped sintered samples, with Pt electrodes vacuum-deposited on both flat surfaces, were used for all the impedance spectroscopy measurements.

3. Results

3.1. Crystallographic Study. In Figure 1, the evolution of the powder X-ray diffraction patterns of the $La_2Mo_2O_{9-0.5x}F_x$ system as the function of the fluorine content is shown. Several peaks in the powder diffraction patterns of compounds with high fluorine content show clear splitting. We carried out Reitveld refinements on the powder X-ray diffraction data of the $La_2Mo_2O_{9-0.5x}F_x$ system. An average structural model, deduced from that of β-$La_2Mo_2O_9$ for fitting the powder X-ray diffraction data of α-$La_2Mo_2O_9$,[2] was used for the Rietveld refinements for all the compositions of the $La_2Mo_2O_{9-0.5x}F_x$ system. This approximate structural

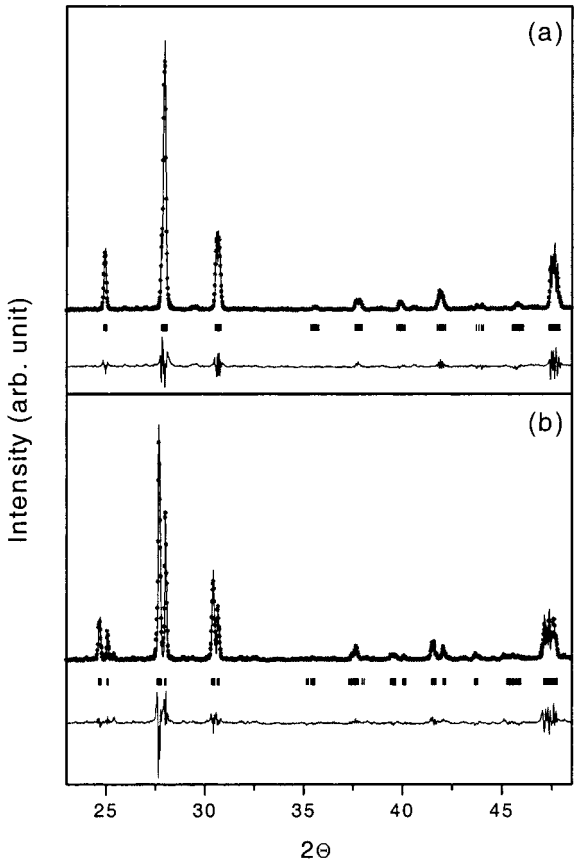

Figure 2. Selected ranges of the powder X-ray diffraction pattern of the (a) α-$La_2Mo_2O_9$ and (b) $La_2Mo_2O_{8.90}F_{0.20}$ phase. In the figure the calculated and the difference plots are also shown.

model does not take into account the superstructure but only the monoclinic distortion and corresponds to the average model for the small monoclinic cell. In Figure 2 we show a selected range of the powder X-ray diffraction patterns of the α-$La_2Mo_2O_9$ and $La_2Mo_2O_{8.90}F_{0.20}$ phases. In the figure the calculated and the difference plots are also shown. A reasonably good fit of the powder diffraction patterns was observed in the cases of all the $La_2Mo_2O_{9-0.5x}F_x$ compositions. In Figure 3a,b we show the evolution of the cell parameters for the $La_2Mo_2O_{9-0.5x}F_x$ system as a function of the fluorine content. In Figure 3a two distinct regions can be seen. Parts b and c in Figure 3 show the variation of the monoclinic angle β and the cell volume with the fluorine content, respectively. The monoclinic angle β decreases monotonically, and the cell volume increases with increasing fluorine content. While the increase in cell volume is expected, owing to the replacement of each oxide ion by two fluoride ions, the decrease of the monoclinic angle β to values smaller than 90° for compositions with $x \geq 0.18$ (Figure 3b) deserves further comments. Any transformation of the lattice to keep the β value higher than 90° results in abrupt changes in the *a*, *b*, and *c* parameters when plotted against "*x*" because of the associated transformation of the axes. This could indicate the existence of two different crystal structures among these phases. A dotted line is used in the figure to demarcate the value of "*x*", above which β is lower than 90°.

To investigate the structure further, we carried out electron diffraction studies on selected compositions of

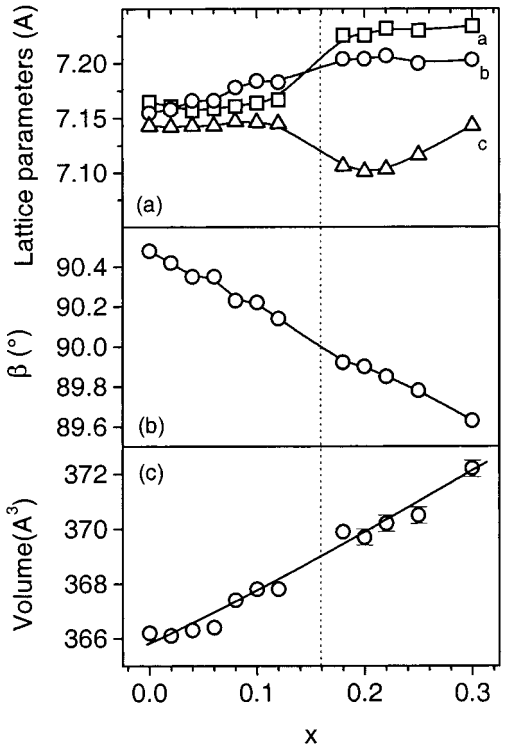

Figure 3. (a) Evolution of the cell parameters *a*, *b*, and *c*; (b) variation of the monoclinic angle β; and (c) variation of the cell volume for the $La_2Mo_2O_{9-0.5x}F_x$ system as a function of the fluorine content "*x*". Error bars exceeding the size of the symbol are shown. The solid lines in the figure are guides to the eye. The dotted line demarcates the value of "*x*" above which β is lower than 90°.

the $La_2Mo_2O_{9-0.5x}F_x$ system. They revealed the presence of superstructures in all these compositions. A statistical analysis of the electron diffraction patterns was carried out to check for any changes in the superstructure with the fluorine content "*x*". The analysis was done on about 20 different crystals for compositions with $x = 0.10$, 0.20, and 0.30. Because of the difficulties involved in the analysis of the superstructure by the reconstruction of the total reciprocal lattice, we have based our statistics on the analysis of the observed basal planes only. For the $x = 0.10$ composition, for a majority of crystals, basal planes with the superstructure 2×3, 3×4, and 2×4 were observed, indicating a $2 \times 3 \times 4$ superstructure, which is the same as that reported for the parent $La_2Mo_2O_9$ composition.[2] For the $x = 0.20$ composition, for a majority of crystals, only basal planes with a superstructure of 3×3 were observed (see Figure 4a), suggesting a $3 \times 3 \times 3$ supercell. For the $x = 0.30$ composition, while for the majority of the crystals we observed basal planes with a 3×3 superstructure, few crystals with other superstructures (e.g., 2×3 and 2×6) were also observed, indicating the less homogeneous nature of this composition. In Figure 4b, we show the electron diffraction pattern showing the 2×6 supercell observed for 1 of the 20 crystals for the $x = 0.30$ composition; it can be interpreted with an extinction condition of the kind $hk0$: $h + k = 2n$.

The results of our X-ray powder diffraction refinements indicate that all the $La_2Mo_2O_{9-0.5x}F_x$ ($x = 0.02-0.30$) compositions can be related to two different structures, distorted to various extents. The electron diffraction study shows the presence of superlattice in

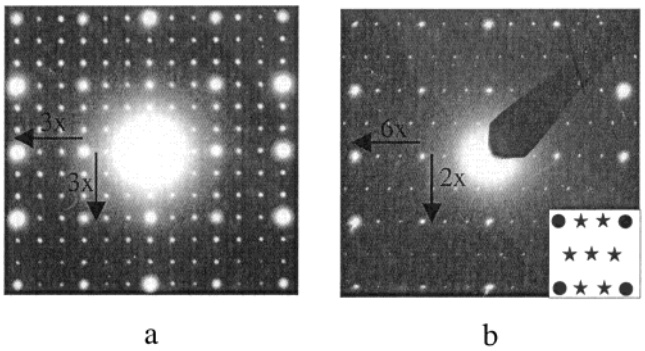

Figure 4. Electron diffraction patterns of (a) $La_2Mo_2O_{8.90}F_{0.20}$ along a crystallographic axis. The arrows are placed along the bright spots corresponding to the small cell. The small spots are due to the 3 × 3 × 3 superstructure; (b) $La_2Mo_2O_{8.85}F_{0.30}$ with the 2 × 6 superstructure. In the inset a schematic drawing of the supercell is shown. In the drawing the solid circle represents the small cell and the stars are used to represent the supercell.

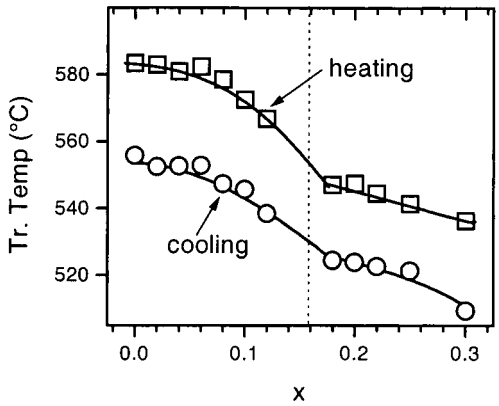

Figure 5. Variation of the transition temperature as found by DTA as the function of the fluorine content in the $La_2Mo_2O_{9-0.5x}F_x$ system. The solid lines are guides to the eye. The dotted line demarcates the two ranges of "*x*" (see text for details).

these compositions, clearly delineating two different superstructures.

3.2. Phase Transition. All the $La_2Mo_2O_{9-0.5x}F_x$ compositions showed the presence of a transition in their DTA plots. Thermal hysteresis was observed in all of them, pointing to the first-order nature of these transitions. In Figure 5 we show the variation of the transition temperature as found by DTA as a function of the fluorine content. With increasing fluorine content the transition temperature decreases. The transition temperature of the $x = 0.30$ sample is 47 °C lower than that of the $x = 0.00$ sample. Notice however that the transition temperature does not decrease uniformly with increasing values of "*x*" and two regions can be delineated as in the crystallographic study. In this Figure a dotted line is drawn at the "*x*" value that demarcates these two regions in the Figure 3.

3.3. Thermal Stability. The thermal stability of the $La_2Mo_2O_{9-0.5x}F_x$ system was checked by DTA and also by a comparison of the powder diffraction patterns recorded at room temperature, after the samples were heated at different high temperatures for 12 h in air. In Figure 6 we show one such set of diffraction patterns of the two compositions $x = 0.1$ and 0.2. The plots also show the diffraction patterns of the "as-prepared"

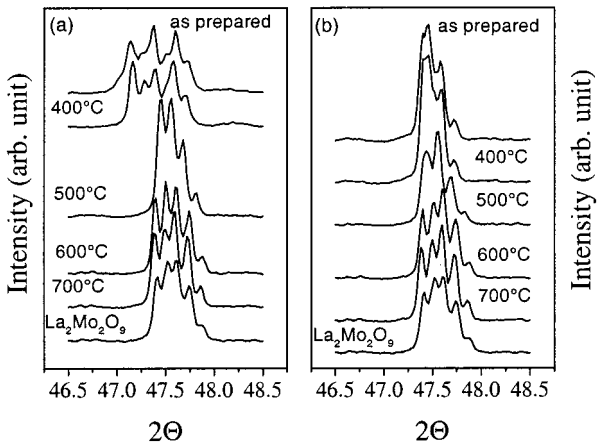

Figure 6. Powder X-ray diffraction pattern of the $La_2Mo_2O_{9-0.5x}F_x$ (left $x = 0.20$; right $x = 0.10$) system recorded after heating them at different temperatures; powder X-ray diffraction patterns of the as-prepared samples and of α-$La_2Mo_2O_9$ are also shown.

compositions and the parent compound $La_2Mo_2O_9$. The diffraction patterns of the "as-prepared" samples and the ones recorded after heating them at high temperatures (≈700 °C) are drastically different. Besides, the diffraction pattern of the "as-prepared" $x = 0.10$ sample resembles that of the $x = 0.20$ sample recorded after it was heated at an intermediate temperature (≈500 °C). Clearly, the $La_2Mo_2O_{9-0.5x}F_x$ system starts loosing its fluorine content when heated above 400 °C for a long duration (≈12 h) of time.

3.4. Anionic Conduction. We carried out impedance spectroscopic analysis of the $La_2Mo_2O_{9-0.5x}F_x$ system in a broad frequency and temperature range. In Figure 7 the impedance spectroscopic data of the parent compound $La_2Mo_2O_9$ recorded at 210 °C are shown. The characteristic semi-circular arc of the Nyquist plot indicated the presence of at least one relaxation process. It is convenient to plot the impedance data as the real part of impedance (Z') vs imaginary part divided by the frequency (Z''/f) as shown in Figure 7a. The linear region in such plots represents a relaxation process, with the slope and the *y*-intercept of the line giving the relaxation frequency and a characteristic resistance, respectively.[6] In Figure 7a the Z' vs Z''/f plot shows two linear regions, indicating the presence of two relaxation processes. In polycrystalline ionic conducting materials the relaxation process could correspond to one of the three: the bulk of the material (f_B), the grain boundary (f_{gb}), or the electrode processes (f_{el}), with $f_B \geq f_{gb} \geq f_{el}$. We did not find any other relaxation process at higher frequencies in the impedance spectra recorded, covering a broad frequency range of 0.10 Hz to 1.8 GHz as well as lower temperatures going down to −150 °C. These experiments prompted us to identify the high-frequency relaxation process of our Z' vs Z''/f plot as due to that of the bulk of the material. It is to be noted that this experiment also points to the likely absence of any electronic contribution to the total conductivity, as one would expect to see the signatures of the relaxation due to electronic conductivity in the broad frequency (0.1 Hz to 1.8 GHz) and temperature (−150−350 °C) ranges

(6) Abrantes, J. C. C.; Labrincha, J. A.; Frade, J. R. *Mater. Res. Bull.* **2000**, *35*, 727.

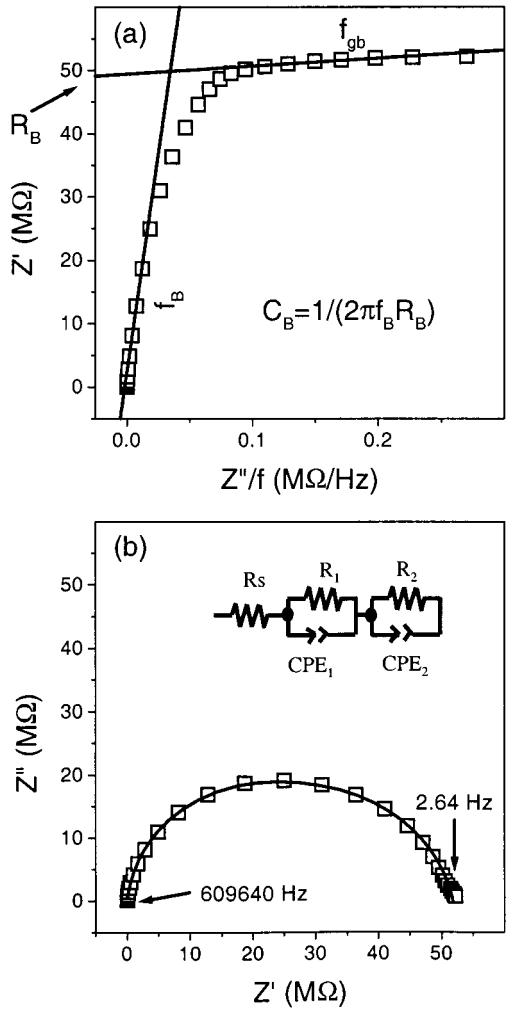

Figure 7. Impedance spectrum of $La_2Mo_2O_9$ recorded at 210 °C; (a) as Z' vs Z''/f representation and (b) in the form of the Nyquist plot. The solid lines in (a) are the fits to the linear regions of the spectrum. The solid line in (b) is the nonlinear fit to the impedance data using an equivalent circuit as shown in the circuit diagram. R represents resistance and CPE represents the constant phase elements. The measured range of frequency is indicated in the figure.

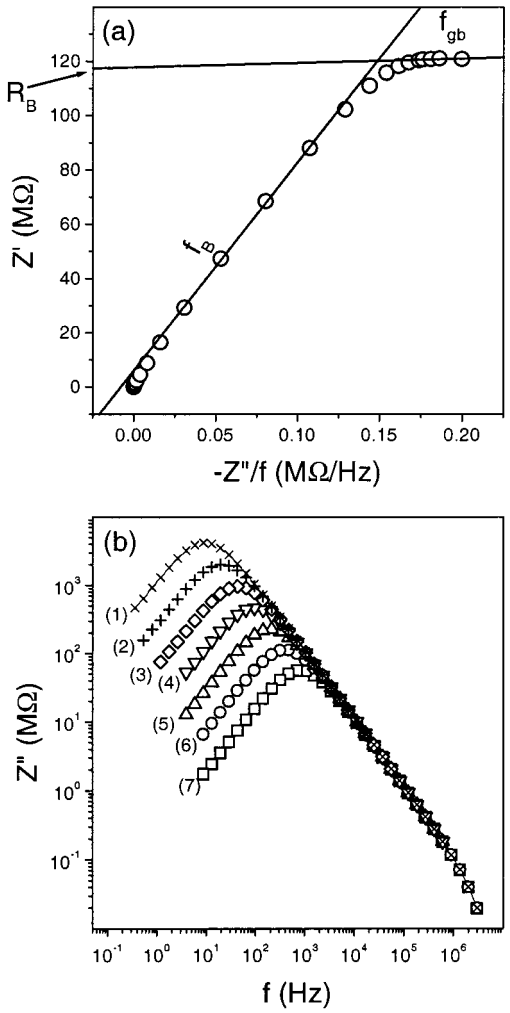

Figure 8. (a) Impedance spectrum of $La_2Mo_2O_{8.95}F_{0.10}$ composition recorded at 200 °C shown in the Z' vs Z''/f representation. (b) Impedance spectra of $La_2Mo_2O_{8.95}F_{0.10}$ composition as Z'' vs f plots recorded at different temperatures; plots labeled (1), (2), (3), (4), (5), (6), and (7) were recorded at 140, 150, 160, 170, 180, 190, and 200 °C, respectively.

covered in our measurements. Calculation of the capacitance using the expression $C = 1/(2\pi fR)$ gives a value (3×10^{-12} F), which is typical of the bulk capacitance of the anionic conductors. With the knowledge that our impedance data have two relaxation processes, we were able to carry out nonlinear curve fitting of these impedance data using a circuit model with two RC components corresponding to the bulk and the grain boundary relaxation of the polycrystalline material[7] (see Figure 7b). The values of the resistance and capacitance obtained by the curve fit compares well with the values obtained from the Z' vs Z''/f plots. We carried out such impedance spectroscopic analysis for the various compositions studied in the $La_2Mo_2O_{9-0.5x}F_x$ system. In Figure 8a we show the impedance spectroscopic data of $La_2Mo_2O_{8.95}F_{0.10}$ recorded at 200 °C in the Z' vs Z''/f representation. Two linear regions in the plot can easily be discerned. In Figure 8b, the Z'' vs f plots for the same composition, obtained at different temperatures, is shown. The maximum (peak) observed in this plot corresponds to the relaxation frequency. With increasing temperature the relaxation frequency shifts to higher values. In fact, the relaxation frequency (f_B) is activated and falls on a straight line when plotted as $\log(f_B)$ vs $1/T$. In parts a and c and parts b and d of Figure 9, the σT vs $1/T$ plots and f_B vs $1/T$ plots for the parent $La_2Mo_2O_9$ and the $La_2Mo_2O_{8.95}F_{0.10}$ compositions are shown, respectively. The activation energy (E_a) as obtained from the σT vs $1/T$ plots match very well with that obtained from the f_B vs $1/T$ plots for both compositions. The same is true for all the compositions studied in the $La_2Mo_2O_{9-0.5x}F_x$ system. This indicates that the relaxation process and the conductivity could be related to the same physical process in this system.

In Table 1, the activation energies (E_a) as obtained from the σT vs $1/T$ and f_B vs $1/T$ plots for selected compositions of the $La_2Mo_2O_{9-0.5x}F_x$ system are listed. We notice that the activation energies of the fluorine-doped lanthanum molybdate systems are higher than that of the parent $La_2Mo_2O_9$ in the measured temperature range of 125−300 °C, which falls much below the transition temperature of any of the compositions studied.

(7) Macdonald, J. R., Ed. *Impedance Spectroscopy: Emphasizing Solid Materials and Systems*; John Wiley and Sons: New York, 1987.

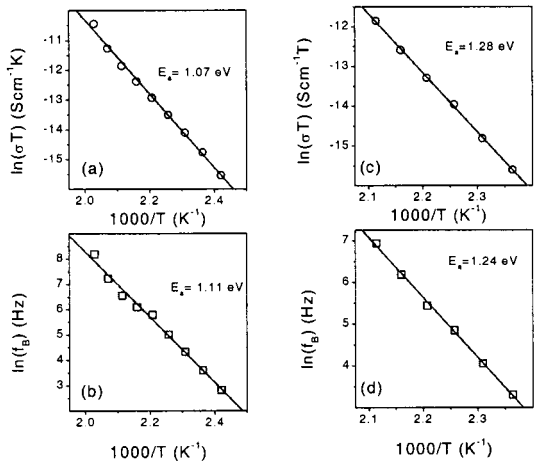

Figure 9. σT vs $1/T$ and f vs $1/T$ plots for $La_2Mo_2O_9$ (left) and $La_2Mo_2O_{8.95}F_{0.10}$ (right).

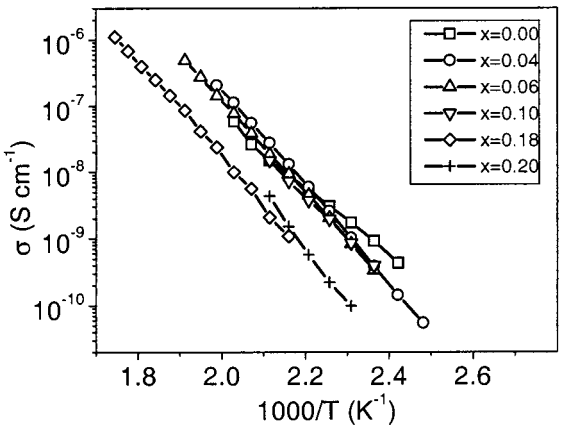

Figure 10. σ vs $1/T$ plots of the $La_2Mo_2O_{9-0.5x}F_x$ system.

Table 1. Activation Energy from the Conductivity (σT) and the Relaxation Frequency (f_B) Data for the $La_2Mo_2O_{9-0.5x}F_x$ System

x	E_a (σT), eV	E_a (f_B), eV	x	E_a (σT), eV	E_a (f_B), eV
0.00	1.07(3)	1.11(4)	0.10	1.28(2)	1.24(3)
0.04	1.43(1)	1.42(2)	0.18	1.49(2)	1.43(3)
0.06	1.39(1)	1.28(2)	0.20	1.58(5)	1.60(3)

In Figure 10 the σ vs $1/T$ plots for selected compositions are shown. We notice that the conductivity plots seem to be falling in two distinct regions. The conductivity of the samples with high fluorine content (x = 0.18,0.20) is lower than that of the samples with lower fluorine content (x = 0.04, 0.06, 0.10). The compositions of these two regions can be mapped on to those in the two distinct regions observed in our lattice parameter plots (Figure 3) and the transition temperature vs "x" plots (Figure 5). Our electron diffraction study showed that the compositions belonging to these two different regions have two different superstructures.

In parts a and b of Figure 11, the σT vs $1/T$ plots in the temperature range of 380−680 °C is shown for the x = 0.00, 0.20 and x = 0.10, 0.30 compositions, respectively. The temperature range of the plots includes the transition temperatures of the respective compositions. A comment on these plots seems essential. All these measurements were carried out under similar conditions. The duration of each experiment was such that the transition temperature of $La_2Mo_2O_9$ was reproducible while our DTA plots showed very small changes in the transition temperatures of the fluorine-doped lanthanum molybdates. These plots show that the fluorine-doped lanthanum molybdate samples exhibit a jump in their conductivity values comparable to that observed in the parent $La_2Mo_2O_9$, but at lower temperatures.

4. Discussions

Like in $La_2Mo_2O_9$, the fluorine-doped lanthanum molybdates show a first-order phase transition from a high-temperature form to a low-temperature form having a distorted lattice. Two distinct regimes with two different ranges of "x" values (range 1: including $0.00 \le x \le 0.12$; range 2: including $0.18 \le x \le 0.30$) could be delineated for the $La_2Mo_2O_{9-0.5x}F_x$ compositions. The $La_2Mo_2O_{9-0.5x}F_x$ compositions have different structures in ranges 1 and 2. In each range the extent of distortion increases with increasing "x" value. The anionic substitution in $La_2Mo_2O_9$ could be contrasted with the substitutions made at the cationic sites. Several experiments involving various substitutions at the La and Mo sites have shown that such substitutions lead to the suppression of the distortion, making the structure of the resulting compound cubic.[4] These substitutions also have the effect of suppressing the first-order transition observed in $La_2Mo_2O_9$ around 580 °C. While a random disorder at the cationic site could cause such an effect, the same is not applicable for the anionic substitutions. The increase in the lattice distortion with increasing fluorine content probably reflects a correlation between the positions occupied by fluoride ions. Clearly, more information on the crystal structures of the $La_2Mo_2O_{9-0.5x}F_x$ compositions is required.

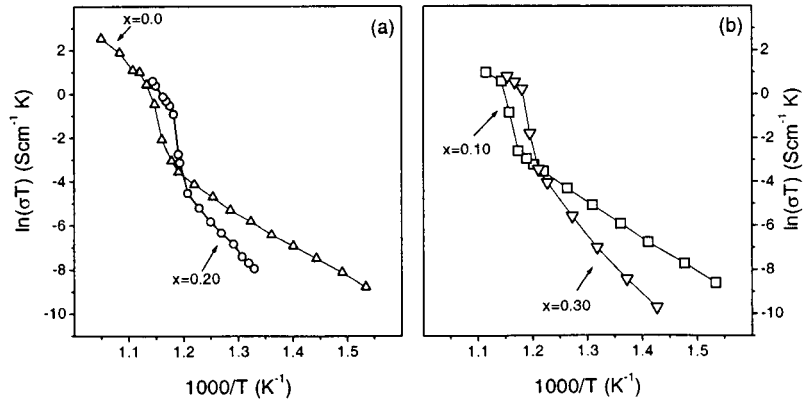

Figure 11. High temperature σT vs $1/T$ plots for $La_2Mo_2O_{9-0.5x}F_x$ compositions: (a) x = 0.00, 0.20 and (b) x = 0.10, 0.30, respectively.

The ionic conductivity of α-$La_2Mo_2O_9$ is much lower than that of the β-$La_2Mo_2O_9$ phase. In the $La_2Mo_2O_{9-0.5x}F_x$ system, the conductivity in the temperature range of 125−300 °C is lower for compositions of range 2 ($x = 0.20, 0.18$) than for the compositions of range 1 ($x = 0.10, 0.06, 0.04$) (see Figure 10). The $La_2Mo_2O_{9-0.5x}F_x$ compositions show a jump in their conductivity value around the first-order transition temperature, comparable to that of $La_2Mo_2O_9$. Hence, the decrease in the transition temperature with increasing fluorine content is a significant phenomenon. The loss of fluorine content from the $La_2Mo_2O_{9-0.5x}F_x$ system when heated to high temperature for long durations is a drawback; however, the effect of such a loss of fluorine content on various physical properties of the system including the first-order phase transition temperature and the ionic conductivity can be clearly seen with good certainty from our experiments. Significantly, partial substitution of fluorine in a system like $La_2Mo_2O_9$ exhibiting an order−disorder type of transition (with a low *T* distorted to a high *T* disordered phase transition and a simultaneous jump in its anionic conductivity) can be considered as a way to decrease the transition temperature.

From our experiments it is not obvious if the fluoride ions take part in ionic conduction but it is clear that they take part in modifying the crystallographic as well as the transport properties of the system, leading to higher conductivity at temperatures lower than the transition temperature of the parent $La_2Mo_2O_9$ compound.

Acknowledgment. The authors thank A. M. Mercier for her help in the sealed Pt tube experiments.

CM011239X